

# Bayesian analysis of anisotropic cosmologies: Bianchi VII<sub>h</sub> and WMAP

J. D. McEwen<sup>1,2\*</sup>, T. Josset<sup>1,3,4†</sup>, S. M. Feeney<sup>1,‡</sup>, H. V. Peiris<sup>1§</sup> and A. N. Lasenby<sup>5¶</sup>

<sup>1</sup>*Department of Physics and Astronomy, University College London, London WC1E 6BT, U.K.*

<sup>2</sup>*Mullard Space Science Laboratory (MSSL), University College London, Surrey RH5 6NT, U.K.*

<sup>3</sup>*Ecole Normale Supérieure de Cachan, 94230 Cachan, France*

<sup>4</sup>*Université Pierre et Marie Curie, 75005 Paris, France*

<sup>5</sup>*Astrophysics Group, Cavendish Laboratory, Madingley Road, Cambridge CB3 0HE, U.K.*

Accepted —. Received —; in original form —

## ABSTRACT

We perform a definitive analysis of Bianchi VII<sub>h</sub> cosmologies with WMAP observations of the cosmic microwave background (CMB) temperature anisotropies. Bayesian analysis techniques are developed to study anisotropic cosmologies using full-sky and partial-sky, masked CMB temperature data. We apply these techniques to analyse the full-sky internal linear combination (ILC) map and a partial-sky, masked W-band map of WMAP 9-year observations. In addition to the physically motivated Bianchi VII<sub>h</sub> model, we examine phenomenological models considered in previous studies, in which the Bianchi VII<sub>h</sub> parameters are decoupled from the standard cosmological parameters. In the two phenomenological models considered, Bayes factors of 1.7 and 1.1 units of log-evidence favouring a Bianchi component are found in full-sky ILC data. The corresponding best-fit Bianchi maps recovered are similar for both phenomenological models and are very close to those found in previous studies using earlier WMAP data releases. However, no evidence for a phenomenological Bianchi component is found in the partial-sky W-band data. In the physical Bianchi VII<sub>h</sub> model we find no evidence for a Bianchi component: WMAP data thus do not favour Bianchi VII<sub>h</sub> cosmologies over the standard  $\Lambda$  Cold Dark Matter ( $\Lambda$ CDM) cosmology. It is not possible to discount Bianchi VII<sub>h</sub> cosmologies in favour of  $\Lambda$ CDM completely, but we are able to constrain the vorticity of physical Bianchi VII<sub>h</sub> cosmologies at  $(\omega/H)_0 < 8.6 \times 10^{-10}$  with 95% confidence.

**Key words:** cosmology: cosmic background radiation – cosmology: observations – methods: data analysis – methods: statistical.

## 1 INTRODUCTION

The  $\Lambda$  Cold Dark Matter ( $\Lambda$ CDM) cosmological concordance model has recently emerged as an accurate description of our Universe. In this model the current Universe is dominated by dark energy and dark matter, with structure seeded by primordial density perturbations generated during an inflationary phase in the early Universe. Support for  $\Lambda$ CDM is derived from a range of recent high-precision cosmological observations, with measurements of the cosmic microwave background (CMB), in particular those made by the Wilkinson Microwave Anisotropy Probe (WMAP) (Komatsu et al. 2011; Larson et al. 2011; Hinshaw et al. 2012), playing a leading role. While the concordance model is undeniably successful, it is important to test the assumptions on which it is

based. One of the most fundamental assumptions of  $\Lambda$ CDM cosmology is the cosmological principle; namely, that the Universe is homogenous and isotropic on large scales. Evidence that this assumption is inaccurate would necessitate revision of  $\Lambda$ CDM.

In this article we seek to test the global isotropy of the Universe. When studying phenomena beyond cosmological concordance it is important to do so in the context of a well-motivated cosmological model. We focus on the homogenous but anisotropic Bianchi models. In these models the assumption of isotropy about each point in the Universe is relaxed, yielding more general solutions to Einstein’s field equations. For small anisotropy, as demanded by current observations, linear perturbation about the standard Friedmann-Robertson-Walker (FRW) metric may be applied, leading to a subdominant, deterministic contribution to the CMB fluctuations. In this setting CMB fluctuations may be viewed as the sum of a deterministic Bianchi contribution and the usual stochastic contribution that arises in the  $\Lambda$ CDM model.

\* jason.mcewen@ucl.ac.uk

† tjosset@ens-cachan.fr

‡ stephen.feeney.09@ucl.ac.uk

§ h.peiris@ucl.ac.uk

¶ a.n.lasenby@mrao.cam.ac.uk

The induced CMB temperature fluctuations that result in the homogenous Bianchi models were first studied by [Collins & Hawking \(1973\)](#) and [Barrow et al. \(1985\)](#) (and subsequently [Barrow 1986](#)), ignoring the effects of dark energy. [Barrow et al. \(1985\)](#) focus on the most general Bianchi VII<sub>h</sub> and IX types, corresponding to open/flat and closed universes respectively. Since tight constraints have already been placed on Bianchi IX models by [Barrow et al. \(1985\)](#), we follow the recent trend in the literature and focus on the open/flat Bianchi VII<sub>h</sub> models, in which geodesic focusing produces spiral-type contributions in the CMB. Although we focus on CMB temperature fluctuations only in this article, we note that the CMB polarisation contributions induced in Bianchi models have also been studied recently ([Pontzen & Challinor 2007](#); [Pontzen 2009](#); [Pontzen & Challinor 2011](#)).

Bianchi VII<sub>h</sub> models were first compared to COBE data by [Bunn et al. \(1996\)](#) and [Kogut et al. \(1997\)](#), and to WMAP data by [Jaffe et al. \(2005, 2006b\)](#). A statistically significant correlation between one of the Bianchi VII<sub>h</sub> models and the WMAP internal linear combination (ILC) map ([Bennett et al. 2003](#)) was discovered by [Jaffe et al. \(2005\)](#) by modelling the CMB as an unknown Bianchi component on top of the (fixed) best-fit WMAP  $\Lambda$ CDM cosmology. However, it was noted that the parameters of the best-fit Bianchi component were incompatible with those of  $\Lambda$ CDM. Nevertheless, quite remarkably it was found that when the WMAP data were ‘corrected’ for the best-fit Bianchi map, some of the so-called ‘anomalies’ reported in WMAP data disappeared ([Jaffe et al. 2005, 2006b](#); [Cayon et al. 2006](#); [McEwen et al. 2006](#)). A modified template-fitting technique was performed by [Land & Magueijo \(2006\)](#) and, although a statistically significant template fit was not reported, the corresponding ‘corrected’ WMAP data were again free of many large scale ‘anomalies’. Subsequently, [Ghosh et al. \(2007\)](#) used the bipolar power spectrum of WMAP data to constrain the amplitude of any Bianchi component in the CMB.

Following this renewed interest in Bianchi models, the CMB temperature fluctuations induced in Bianchi VII<sub>h</sub> models incorporating dark energy were derived by [Jaffe et al. \(2006c\)](#) and [Bridges et al. \(2007\)](#) (and subsequently by [Pontzen & Challinor \(2007\)](#), [Pontzen \(2009\)](#) and [Pontzen & Challinor \(2011\)](#), where recombination is treated in a more sophisticated manner and reionisation is supported). In this scenario, a degeneracy between the matter and dark energy densities,  $\Omega_m$  and  $\Omega_\Lambda$  respectively, is introduced, but the cosmological parameters of the best-fit Bianchi template found in WMAP data nevertheless remain inconsistent with constraints from the CMB alone ([Jaffe et al. 2006a,c](#)). Furthermore, [Pontzen & Challinor \(2007\)](#) compared the polarisation power spectra of the best-fit Bianchi VII<sub>h</sub> model found by [Jaffe et al. \(2006a\)](#) with the WMAP 3-year data ([Page et al. 2007](#)) and also concluded that the model could be ruled out since it produced greater polarization than observed in the WMAP data. A Bayesian analysis of Bianchi VII<sub>h</sub> models was performed by [Bridges et al. \(2007\)](#) using WMAP ILC data to explore the joint cosmological and Bianchi parameter space via Markov chain Monte Carlo sampling. The  $\Omega_m$ - $\Omega_\Lambda$  degeneracy of Bianchi VII<sub>h</sub> models was studied more thoroughly and, although a similar best-fit Bianchi template was found in WMAP data, it was again determined that the parameters of the resulting Bianchi cosmology were inconsistent with standard constraints. In a following study by [Bridges et al. \(2008\)](#) it was suggested that the CMB ‘cold spot’ ([Vielva et al. 2004](#); [Cruz et al. 2006](#); [Vielva 2010](#)) could be driving the best-fit Bianchi component found in WMAP data.

In this article we perform a definitive study of Bianchi VII<sub>h</sub> cosmologies with WMAP temperature data. We develop a Bayesian analysis technique capable of studying Bianchi models using

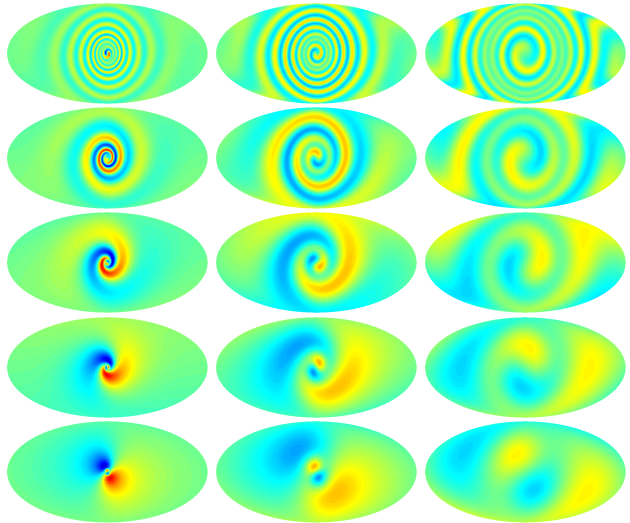


**Figure 1.** Simulated deterministic CMB temperature contributions in Bianchi VII<sub>h</sub> cosmologies for varying  $x$  and  $\Omega_{\text{total}}$  (left-to-right  $\Omega_{\text{total}} \in \{0.10, 0.50, 0.95\}$ ; top-to-bottom  $x \in \{0.1, 0.3, 0.7, 1.5, 6.0\}$ ). In these maps the spiral pattern typical of Bianchi VII<sub>h</sub> induced temperature fluctuations is rotated from the South pole to the Galactic centre for illustrational purposes. The parameter values  $\kappa = +1$  and  $(\alpha, \beta, \gamma) = (0^\circ, -90^\circ, 0^\circ)$  were also set when generating these simulations.

partial-sky CMB observations, allowing us for the first time to study individual WMAP bands rather than the ILC map, which was not originally intended for cosmological analysis ([Bennett et al. 2003](#)). We sample the complete set of parameters describing the  $\Lambda$ CDM cosmology and the Bianchi VII<sub>h</sub> model simultaneously, and perform the first rigorous study of the physically motivated scenario where the parameters of the Bianchi model are coupled to the standard cosmology. To make comparisons with previous work, we also consider the non-physical scenario where the Bianchi parameters are decoupled from the standard cosmological parameters. We employ the latest (and final) 9-year release of WMAP observations (previous studies have considered WMAP 1- and 3-year data only), and perform a Bayesian model-selection analysis of Bianchi VII<sub>h</sub> models, using nested sampling methods ([Skilling 2004](#); [Feroz & Hobson 2008](#); [Feroz et al. 2009](#)), to determine whether WMAP data suggest we inhabit an anisotropic Bianchi VII<sub>h</sub> universe instead of a standard isotropic  $\Lambda$ CDM universe.

The remainder of this article is structured as follows. In Sec. 2 we briefly review Bianchi VII<sub>h</sub> cosmologies. We describe the Bayesian analysis techniques that we develop to study full- and partial-sky CMB observations in Sec. 3. Although focus is given to Bianchi models, these techniques are generic and may be used to study other general anisotropic cosmologies. In Sec. 4 we apply our analysis to WMAP 9-year data to constrain Bianchi VII<sub>h</sub> cosmologies. Concluding remarks are made in Sec. 5.

## 2 BIANCHI VII<sub>h</sub> COSMOLOGIES

In this section we review Bianchi VII<sub>h</sub> cosmologies, focusing on their description; we defer technical details to [Barrow et al. \(1985\)](#) and [Jaffe et al. \(2006c\)](#). Note that we adopt the solutions to the temperature fluctuations induced in Bianchi VII<sub>h</sub> models when incorporating dark energy, as derived by [Lasenby](#) and also adopted by [Bridges et al. \(2007\)](#).

Bianchi VII<sub>h</sub> models contain a free parameter, usually denoted  $x$ , as first identified by Collins & Hawking (1973). This parameter is related to the  $h$  parameter of type VII<sub>h</sub> models by

$$x = \sqrt{\frac{h}{1 - \Omega_{\text{total}}}}, \quad (1)$$

where the total energy density  $\Omega_{\text{total}} = \Omega_{\text{m}} + \Omega_{\Lambda}$ . Physically,  $x$  is related to the characteristic wavelength over which the principle axes of shear and rotation change orientation. Consequently,  $x$  acts to change the ‘tightness’ of the spiral-type CMB temperature contributions that are typical of Bianchi VII<sub>h</sub> cosmologies. Bianchi VII<sub>h</sub> models are also described by their shear modes  $(\sigma_{12}/H)_0$  and  $(\sigma_{13}/H)_0$ , vorticity  $(\omega/H)_0$ , and handedness  $\kappa$ , where  $H$  is the Hubble parameter. The handedness parameter takes the values  $\kappa = +1$  and  $\kappa = -1$  for maps with right- and left-handed spirals respectively. Vorticity is related to the other parameters by (Barrow et al. 1985)

$$\left(\frac{\omega}{H}\right)_0 = \frac{(1+h)^{1/2}(1+9h)^{1/2}}{6x^2\Omega_{\text{total}}} \sqrt{\left(\frac{\sigma_{12}}{H}\right)_0^2 + \left(\frac{\sigma_{13}}{H}\right)_0^2}. \quad (2)$$

The spherical harmonic coefficients of the Bianchi VII<sub>h</sub> induced temperature component are proportional to  $[(\sigma_{12} \pm i\sigma_{13})/H]_0$  and are non-zero for azimuthal modes  $m = \mp 1$  only (Barrow et al. 1985; McEwen et al. 2006; Pontzen & Challinor 2007). Hence, varying the phase of  $\sigma_{12} + i\sigma_{13}$  corresponds to an azimuthal rotation, *i.e.* a change of coordinates, while the rotationally invariant part depends on  $\sigma_{12}^2 + \sigma_{13}^2$ , and we are thus free to choose equality of shear modes  $\sigma = \sigma_{12} = \sigma_{13}$  (Pontzen & Challinor 2007), which we do for consistency with previous studies (*e.g.* Jaffe et al. 2005). The amplitude of deterministic Bianchi VII<sub>h</sub> temperature maps may be characterised by either  $(\sigma/H)_0$  or  $(\omega/H)_0$  since these parameters influence the amplitude of the map only and not its morphology.

Since the CMB temperature fluctuations induced in Bianchi VII<sub>h</sub> models are anisotropic on the sky, the orientation of the CMB contribution may vary also, introducing three additional degrees-of-freedom. The orientation of a map representing the Bianchi VII<sub>h</sub> CMB fluctuations is described by the Euler angles<sup>1</sup>  $(\alpha, \beta, \gamma)$ , where for  $(\alpha, \beta, \gamma) = (0^\circ, 0^\circ, 0^\circ)$  the spiral pattern typical of Bianchi VII<sub>h</sub> temperature fluctuations is centred on the South pole. To summarise, Bianchi VII<sub>h</sub> models may be described by the parameter vector  $\Theta_{\text{B}} = (\Omega_{\text{m}}, \Omega_{\Lambda}, x, (\omega/H)_0, \alpha, \beta, \gamma)$  (note that we do not include the handedness parameter  $\kappa$  in  $\Theta_{\text{B}}$  since this is used to distinguish between left- and right-handed models).

In the analysis performed herein the BIANCHI2<sup>2</sup> code is used to simulate the temperature fluctuations induced in Bianchi VII<sub>h</sub> models. Bianchi VII<sub>h</sub> models induce only large scale temperature fluctuations in the CMB and, consequently, the resulting Bianchi maps have a low band-limit both globally and azimuthally, *i.e.* in both  $\ell$  and  $m$  in spherical harmonic space; indeed, only those harmonic coefficients with  $m = \pm 1$  are non-zero (Barrow et al. 1985). In the BIANCHI2 code Bianchi VII<sub>h</sub> temperature fluctuations may be computed directly in either real or harmonic space. In the analysis performed herein we compute temperature fluctuations directly in harmonic space to avoid any pixelisation artefacts and since the resulting temperature fluctuations can be rotated accurately and efficiently in harmonic space (see McEwen et al.

2006) due to their low azimuthal band-limit. Examples of simulated Bianchi VII<sub>h</sub> temperature maps are illustrated in Fig. 1 for a range of parameters.

### 3 BAYESIAN ANALYSIS OF ANISOTROPIC COSMOLOGIES

We describe in this section a generic methodology to perform a Bayesian analysis of anisotropic cosmologies using CMB observations. Since we are motivated by the analysis of Bianchi VII<sub>h</sub> cosmologies, we consider a deterministic global template and pose the analysis in harmonic space (where Bianchi VII<sub>h</sub> contributions can be computed accurately and rotated efficiently). The extension to alternative settings, such as non-trivial topologies (Niarchou et al. 2003; Cornish et al. 2004; Dineen et al. 2005; Kunz et al. 2006; Bielewicz & Riazuelo 2009), is also highlighted. Firstly, we describe a generic Bayesian analysis of anisotropic cosmologies, before restricting this to the specific settings of full- and partial-sky CMB observations. Finally, we perform simulations to validate the implementation of the methodology presented.

#### 3.1 Bayesian analysis

By Bayes’ theorem we may write the posterior distribution of the parameters  $\Theta$  of our model of interest  $M$ , given data  $\mathbf{d}$ , as

$$P(\Theta | \mathbf{d}, M) = \frac{P(\mathbf{d} | \Theta, M) P(\Theta | M)}{P(\mathbf{d} | M)} \propto P(\mathbf{d} | \Theta, M) P(\Theta | M), \quad (3)$$

where  $P(\mathbf{d} | \Theta, M)$  is the likelihood,  $P(\Theta | M)$  is the prior distribution of the parameters of the model, and  $P(\mathbf{d} | M)$  is the Bayesian evidence, which normalises the posterior distribution. The (unnormalised) posterior distribution encodes our inferred knowledge of the parameters of the model, given the observational data.

We consider both models that include a Bianchi VII<sub>h</sub> contribution in addition to a stochastic CMB component and those that do not. We consider open and flat cosmologies where the cosmological parameters are given by  $\Theta_{\text{C}} = (A_s, n_s, \tau, \Omega_b h^2, \Omega_c h^2, \Omega_{\Lambda}, \Omega_k)$ , where  $A_s$  is the amplitude of the primordial power spectrum,  $n_s$  is the scalar spectral index,  $\tau$  is the optical depth of reionisation,  $\Omega_b h^2$  is the physical baryon density,  $\Omega_c h^2$  is the physical cold dark matter density,  $\Omega_{\Lambda}$  is the dark energy density,  $\Omega_k$  is the curvature density and  $H = 100 h$ ; for the flat case  $\Omega_k = 0$  and we recover the standard six parameter model. For the models including a Bianchi VII<sub>h</sub> contribution, we consider the physical case where the Bianchi parameters  $\Theta_{\text{B}}$  and cosmological parameters  $\Theta_{\text{C}}$  are coupled (*i.e.* where the cosmological density parameters shared by  $\Theta_{\text{B}}$  and  $\Theta_{\text{C}}$  are set equal) and also the non-physical case where they are not (the latter case is considered to make comparisons with previous work). The Bianchi VII<sub>h</sub> parameters  $\Theta_{\text{B}}$  are described in Sec. 2.

For the case where a Bianchi VII<sub>h</sub> template is embedded in a stochastic CMB background described by its power spectrum  $C_l(\Theta_{\text{C}})$ , the likelihood is given by

$$P(\mathbf{d} | \Theta_{\text{B}}, \Theta_{\text{C}}) \propto \frac{1}{\sqrt{|\mathbf{X}(\Theta_{\text{C}})|}} \exp\left[-\chi^2(\Theta_{\text{C}}, \Theta_{\text{B}})/2\right], \quad (4)$$

where

$$\chi^2(\Theta_{\text{C}}, \Theta_{\text{B}}) = [\mathbf{d} - \mathbf{b}(\Theta_{\text{B}})]^{\dagger} \mathbf{X}^{-1}(\Theta_{\text{C}}) [\mathbf{d} - \mathbf{b}(\Theta_{\text{B}})], \quad (5)$$

and where  $\mathbf{b}(\Theta_{\text{B}})$  is the deterministic Bianchi VII<sub>h</sub> template and  $\mathbf{X}(\Theta_{\text{C}})$  is the covariance matrix of the stochastic CMB component (and any noise component included in the model). Eqn. (4) and

<sup>1</sup> The active  $zyz$  Euler convention is adopted, corresponding to the rotation of a physical body in a *fixed* coordinate system about the  $z$ ,  $y$  and  $z$  axes by  $\gamma$ ,  $\beta$  and  $\alpha$  respectively.

<sup>2</sup> <http://www.jasonmcewen.org/>

Eqn. (5) are written in a generic manner, where the likelihood may be given either in real or harmonic space. Since Bianchi VII<sub>h</sub> templates can be computed accurately and rotated efficiently in harmonic space, we specialise to a harmonic space representation, where the data and Bianchi template are given by their spherical harmonic coefficients:  $\mathbf{d} = \{d_{\ell m}\}$  and  $\mathbf{b}(\Theta_B) = \{b_{\ell m}(\Theta_B)\}$ , respectively, considered up to the harmonic band-limit  $\ell_{\max}$ . The covariance matrix  $\mathbf{X}(\Theta_C)$  is then also specified in harmonic space but differs depending on whether the full- or partial-sky setting is considered (we consider each setting in turn in subsequent subsections). For the full-sky setting the covariance matrix is diagonal, whereas this is not the case for the partial-sky setting (assuming isotropic noise in both settings).

We have so far considered the setting where a subdominant, deterministic template is embedded in a stochastic CMB background. However, it is straightforward to extend the analysis to the setting where an anisotropic cosmology does not induce an embedded deterministic template, but rather alters the covariance structure of the stochastic CMB component; this is the case for non-trivial topologies (e.g. Niarchou et al. 2003; Cornish et al. 2004; Dineen et al. 2005; Kunz et al. 2006; Bielewicz & Riazuelo 2009). This setting can be handled in the current framework simply by setting the template component to zero and by replacing the covariance matrix  $\mathbf{X}(\Theta_C)$  with the appropriate covariance matrix for the anisotropic cosmology. The coordinate orientation is again arbitrary in this setting, hence the covariance matrix, or similarly the data, must be varied over all three-dimensional orientations as specified by the Euler angles. In this setting the  $\chi^2$  of the likelihood is written

$$\chi^2(\Theta_A) = \mathbf{d}^\dagger(\alpha, \beta, \gamma) \mathbf{X}^{-1}(\Theta_A) \mathbf{d}(\alpha, \beta, \gamma), \quad (6)$$

where  $\Theta_A$  is the full set of parameters of the anisotropic cosmology and  $\mathbf{d}(\alpha, \beta, \gamma)$  denotes the data rotated by Euler angles  $(\alpha, \beta, \gamma)$ . Since we focus on Bianchi cosmologies here, we consider only the likelihood with  $\chi^2$  given by Eqn. (5) in the remainder of this article.

To determine whether the inclusion of a Bianchi VII<sub>h</sub> component better describes the data the Bayesian evidence is examined, given by

$$E = P(\mathbf{d} | M) = \int d\Theta P(\mathbf{d} | \Theta, M) P(\Theta | M). \quad (7)$$

Using the Bayesian evidence to distinguish between models naturally incorporates Occam's razor, trading off model simplicity and accuracy. The odds ratio between two models  $M_1$  and  $M_2$  may be written in terms of the Bayesian evidences of the models ( $E_1$  and  $E_2$  respectively) by

$$\frac{P(M_1 | \mathbf{d})}{P(M_2 | \mathbf{d})} = \frac{E_1 P(M_1)}{E_2 P(M_2)}. \quad (8)$$

In the absence of any prior information about a preferred model, *i.e.* when  $P(M_1) = P(M_2)$ , the Bayes factor given by the ratio of Bayesian evidences  $E_1/E_2$  is thus identical to the ratio of the model probabilities given the data. Consequently, the Bayes factor may be used to distinguish models in this setting.

The Jeffreys scale (Jeffreys 1961) is often used as a rule-of-thumb when comparing models via their Bayes factor. The log-Bayes factor  $\Delta \ln E = \ln(E_1/E_2)$  represents the degree by which model  $M_1$  is favoured over model  $M_2$ , assuming the models are equally likely *a priori*. On the Jeffreys scale log-Bayes factors are given the following interpretation:  $0 \leq \Delta \ln E < 1$  is regarded as inconclusive;  $1 \leq \Delta \ln E < 2.5$  as significant;  $2.5 \leq \Delta \ln E < 5$  as strong; and  $\Delta \ln E \geq 5$  as conclusive (without loss of generality we have assumed  $E_1 \geq E_2$ ). For reference, a log-Bayes factor of 2.5

corresponds to odds of approximately 1 in 12, while a factor of 5 corresponds to odds of approximately 1 in 150.

### 3.2 Full-sky analysis

In the full-sky setting the covariance matrix is given by  $\mathbf{X}(\Theta_C) = \mathbf{C}(\Theta_C)$ , where  $\mathbf{C}(\Theta_C)$  is the diagonal CMB covariance matrix with entries given by the power spectrum  $C_\ell(\Theta_C)$  on its diagonal. A Bayesian analysis in this setting was first considered by Bridges et al. (2007). To expose the detail of the analysis we make the likelihood explicit in this setting. The likelihood, in terms of the spherical harmonic coefficients of the data  $d_{\ell m}$  and Bianchi VII<sub>h</sub> template  $b_{\ell m}(\Theta_B)$ , is given by

$$P(\{d_{\ell m}\} | \Theta_B, \Theta_C) \propto \prod_{\ell=0}^{\ell_{\max}} \frac{1}{\sqrt{C_\ell(\Theta_C)}} \exp\left\{-\frac{[d_{\ell 0} - b_{\ell 0}(\Theta_B)]^2}{C_\ell(\Theta_C)}\right\} \\ \times \prod_{m=1}^{\ell} \frac{2}{C_\ell(\Theta_C)} \exp\left\{-\frac{|d_{\ell m} - b_{\ell m}(\Theta_B)|^2}{C_\ell(\Theta_C)}\right\}. \quad (9)$$

In practice, it is more convenient numerically to work with the log-likelihood function, given by

$$\ln[P(\{d_{\ell m}\} | \Theta_B, \Theta_C)] \propto \sum_{\ell=0}^{\ell_{\max}} \left\{ (2\ell + 1) \ln[C_\ell(\Theta_C)] \right. \\ \left. + \frac{[d_{\ell 0} - b_{\ell 0}(\Theta_B)]^2}{C_\ell(\Theta_C)} + \frac{2}{C_\ell(\Theta_C)} \sum_{m=1}^{\ell} |d_{\ell m} - b_{\ell m}(\Theta_B)|^2 \right\}. \quad (10)$$

In the case of a zero Bianchi component  $\mathbf{b}(\Theta_B) = 0$ , Eqn. (10) reduces to the log-likelihood function used commonly to compute parameter estimates from the power spectrum estimated from CMB data (e.g. Verde et al. 2003).

### 3.3 Partial-sky analysis

In the partial-sky setting a mask is applied in real space to excise contaminated regions of the data (due to point-source or Galactic contamination, for example). See, for example, the mask applied to simulated CMB data in Fig. 4(a).

Various approaches can be adopted to deal with partial-sky data. The standard approach is to multiply the map by a binary mask. In this setting, the application of a mask induces coupling of harmonic space modes in the resultant data, which can be viewed as a convolution of the original covariance matrix and the mask transfer function in harmonic space (the so-called coupling matrix). This coupling can then be taken into account when making a comparison with theory (e.g. Hivon et al. 2002; Hinshaw et al. 2003). However, we take a different approach here, which avoids the need to compute the coupling matrix explicitly (thereby avoiding the computation of Wigner 3-*j* symbols).

We effectively consider full-sky data but add *masking noise* to marginalise over the pixel values of the data in the masked region. Gaussian masking noise  $m$  is added to the data  $d$  in real space:

$$s(\omega) = d(\omega) + m(\omega), \quad (11)$$

where  $\omega$  denotes angular coordinates on the sphere. The masking noise is chosen to be zero-mean and large in the masked region of the data (*i.e.* zeros of the mask), and zero elsewhere. Consequently, the masking noise is anisotropic over the sky but may be chosen to be uncorrelated, and may thus be defined by its covariance

$$\langle m(\omega_i) m^*(\omega_j) \rangle = \delta_{ij} \sigma_m^2(\omega_i), \quad (12)$$

where  $\delta_{ij}$  is Kronecker delta symbol,  $\omega_i$  denotes the angular coordinate of pixel  $i$ , and the variance of the noise for pixel  $i$  is given by

$$\sigma_m^2(\omega_i) = \begin{cases} \Sigma_m^2, & \omega_i \in \mathbb{M} \\ 0, & \omega_i \in \mathbb{S}^2 \setminus \mathbb{M} \end{cases}, \quad (13)$$

where  $\Sigma_m^2$  is a constant masking noise variance. We adopt the HEALPix (Górski et al. 2005) equal-area pixelisation of the sphere, where the area of each pixel is  $\Omega_{\text{pix}}$ , in order to avoid dealing with pixels of differing areas. Here  $\mathbb{M}$  denotes the masked region of the sky  $\mathbb{S}^2$  and  $\mathbb{S}^2 \setminus \mathbb{M}$  denotes the remaining region. By synthetically adding masking noise that is much larger than the original data in the masked region of the sky, we effectively marginalise over the pixel values of the data in this region. Consequently, only the pixel values of the data outside of the masked region have a large influence on the final analysis. We refer to a particular masking noise realisation as a *noisy mask*. An example noisy mask is shown in Fig. 4(d).

The noisy mask introduces coupling in harmonic space that must be accounted for in the analysis. The effective signal  $s$  to be analysed now includes the original data  $d$  and the noisy mask  $m$ ; thus its covariance is the sum of the covariance of the original data and the noisy mask. The covariance of the noisy mask is given in harmonic space by

$$\mathbf{M}_{\ell m}^{\ell' m'} = \langle m_{\ell m} m_{\ell' m'}^* \rangle \simeq \sum_{\omega_i} \sigma_m^2(\omega_i) Y_{\ell m}^*(\omega_i) Y_{\ell' m'}(\omega_i) \Omega_{\text{pix}}^2, \quad (14)$$

where we have applied Eqn. (12) and again consider signals and their covariance structure in harmonic space (since the analysis of Bianchi VII<sub>h</sub> cosmologies is most accurately and efficiently performed in harmonic space). In Eqn. (14) we approximate the spherical harmonic coefficients of the mask using discrete quadrature:

$$m_{\ell m} = \int_{\mathbb{S}^2} d\Omega(\omega) m(\omega) Y_{\ell m}^*(\omega) \simeq \sum_{\omega_i} \Omega_{\text{pix}} m(\omega_i) Y_{\ell m}^*(\omega_i); \quad (15)$$

note that this is necessarily an approximation since the noisy mask is not band-limited and we adopt the HEALPix (Górski et al. 2005) sampling scheme, which does not admit exact quadrature. Since the underlying data  $d$  and noisy mask  $m$  are independent, the covariance of the effective data  $s$  is given by  $\mathbf{X}(\Theta_C) = \mathbf{C}(\Theta_C) + \mathbf{M}$ , where  $\mathbf{C}(\Theta_C)$  is again the diagonal CMB covariance matrix and  $\mathbf{M}$  is the non-diagonal noisy mask covariance matrix given by Eqn. (14).

To summarise, the partial-sky analysis proceeds as follows. Firstly a zero-mean, Gaussian noisy mask realisation is constructed via Eqn. (12) and Eqn. (13), and its covariance structure is estimated by Eqn. (14). The effective signal under analysis  $s$  is constructed by summing the original data and the noisy mask realisation by Eqn. (11). The Bayesian analysis described in Sec. 3.1 is performed, where the data under analysis is replaced with the effective signal  $s$ , with covariance matrix given by  $\mathbf{X}(\Theta_C) = \mathbf{C}(\Theta_C) + \mathbf{M}$ .<sup>3</sup>

<sup>3</sup> In practice the masked region of the data to be excised will include unknown contamination, rather than a CMB contribution only. Thus, the original data  $d$  are masked before the procedure outlined here is performed. In this setting the covariance matrix  $\mathbf{X}(\Theta_C) = \mathbf{C}(\Theta_C) + \mathbf{M}$  is necessarily an approximation, since the assumption that there is a CMB component in the masked region is no longer valid. However, provided the noise variance  $\Sigma_m^2$  is chosen to be considerably larger than the expected CMB contribution, the approximation is very accurate.

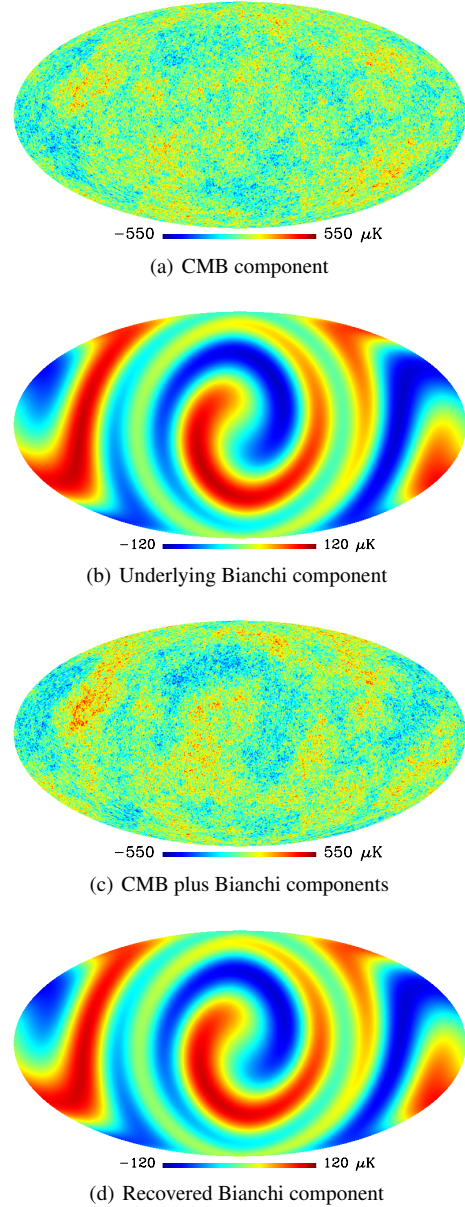


**Figure 2.** Full-sky simulation at  $\ell_{\text{max}} = 512$ . A Bianchi VII<sub>h</sub> component with a large amplitude is simulated (panel b) and embedded in a standard stochastic CMB map (panel a), yielding a resultant CMB plus Bianchi map (panel c) to which a beam and noise are applied. The full-sky Bayesian analysis described in Sec. 3.2 is applied to recover a MAP estimated Bianchi component (panel d). The recovered Bianchi component (panel d) accurately estimates the embedded component (panel b).

### 3.4 Implementation and validation

We have developed the ANICOSMO<sup>4</sup> code to perform a Bayesian analysis of anisotropic cosmologies. The Bayesian analysis described in this section is implemented in ANICOSMO, both in the full- and partial-sky settings. We adopt the MultiNest<sup>5</sup> code (Feroz & Hobson 2008; Feroz et al. 2009) to explore the posterior distribution and to compute Bayesian evidence values, both via nested sam-

<sup>4</sup> The ANICOSMO code will soon be made publicly available from <http://www.jasonmcewen.org/>.

<sup>5</sup> <http://www.mrao.cam.ac.uk/software/multinest/>

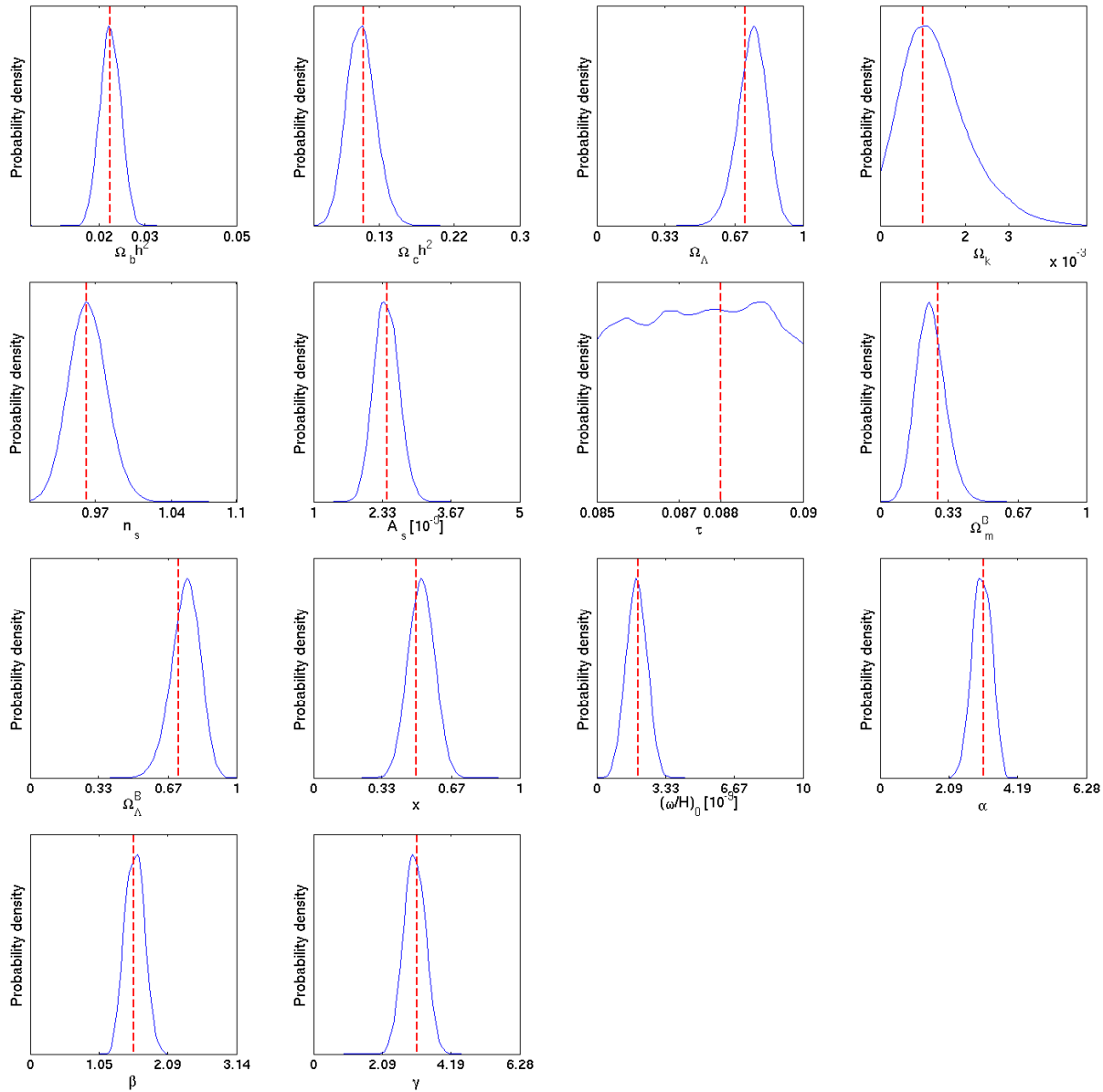


**Figure 3.** Posterior distributions corresponding to the full-sky simulation at  $\ell_{\max} = 512$  shown in Fig. 2. The underlying parameter values of the simulation are indicated by dashed vertical lines. Both cosmological and Bianchi VII<sub>h</sub> parameters are estimated accurately, except for the optical depth of reionisation,  $\tau$ , which is not unexpected when using CMB temperature data alone. For model comparison purposes an unconstrained  $\tau$  does not pose any great concern.

pling (Skilling 2004; Feroz & Hobson 2008; Feroz et al. 2009). The CAMB<sup>6</sup> code (Lewis et al. 2000) is used to compute the CMB power spectrum  $C_\ell(\Theta_C)$  for various cosmological parameters  $\Theta_C$ .

At present the ANICOSMO code is specialised to the study of Bianchi VII<sub>h</sub> cosmologies, where the likelihood is computed through Eqn. (4) and Eqn. (5). However, ANICOSMO may be trivially extended to handle the  $\chi^2$  defined by Eqn. (6) and to study other anisotropic cosmologies, such as non-trivial topologies; this will be the focus of future work.

In the remainder of this subsection we perform simulations to validate the Bayesian analysis method described here and its implementation in the ANICOSMO code. In both the full- and partial-sky settings, we simulate a CMB map and synthetically embed

a simulated Bianchi VII<sub>h</sub> component. To approximate the finite-resolution, noisy measurements of the CMB made by the WMAP experiment (specifically those made in the highest-resolution, 94 GHz W band; Bennett et al. 2012), a Gaussian beam with full-width-half-maximum (FWHM) 13.2' and isotropic noise with power spectrum  $N_\ell = 0.02 (\mu K)^2$  are applied to the simulations. To account for the beam and noise in the Bayesian analysis we simply map  $C_\ell(\Theta_C) \rightarrow b_\ell^2 C_\ell(\Theta_C) + N_\ell$  when computing the CMB covariance matrix and apply the beam to the Bianchi VII<sub>h</sub> template by mapping  $b_{\ell m}(\Theta_B) \rightarrow b_\ell b_{\ell m}(\Theta_B)$ , where  $b_\ell^2$  and  $N_\ell$  are the beam and noise power spectra, respectively. In these simulations we consider the model where the Bianchi parameters  $\Theta_B$  and cosmological parameters  $\Theta_C$  are coupled. Posterior distributions and evidence values are then recovered by ANICOSMO for models including and excluding a coupled Bianchi component in addition to the standard stochastic CMB component. For the purpose of validating the

<sup>6</sup> <http://camb.info/>

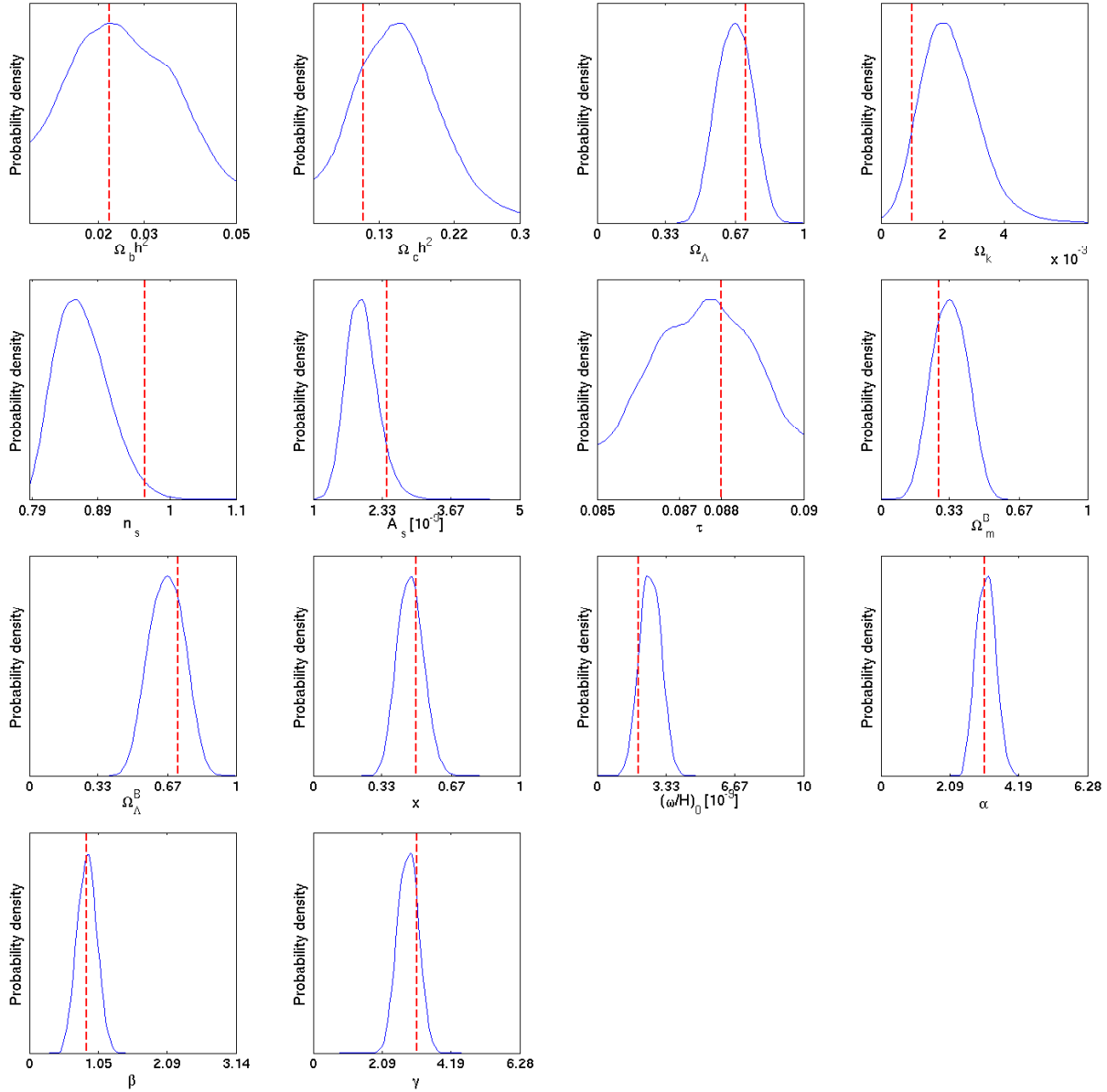


**Figure 5.** Posterior distributions corresponding to the partial-sky simulation at  $\ell_{\max} = 32$  shown in Fig. 4. The underlying parameter values of the simulation are indicated by dashed vertical lines. Both cosmological and Bianchi VII<sub>h</sub> parameters are estimated reasonably well, however since less data is now available due to the lower  $\ell_{\max}$  and masking, the marginalised posterior distributions are not as accurate or well constrained as the full-sky setting, as is to be expected. For model comparison purposes this does not pose any great concern.

implementation, we consider a Bianchi template with a relatively large amplitude of  $(\omega/H)_0 = 2 \times 10^{-9}$ .

Full-sky simulations are shown in Fig. 2. Since the covariance matrix  $\mathbf{X}(\Theta_C)$  is diagonal in this setting, the analysis may be run at high-resolution; hence, we set  $\ell_{\max} = 512$  in this simulation. The *maximum-a-posteriori* (MAP) estimated Bianchi VII<sub>h</sub> component recovered from the peak of the posterior distribution  $P(\Theta | \mathbf{d}, M)$  is shown in Fig. 2(d) and is clearly an accurate estimate of the embedded component shown in Fig. 2(b). The marginalised posterior distributions recovered for each parameter are shown in Fig. 3. Both cosmological and Bianchi VII<sub>h</sub> parameters are estimated accurately, except for the optical depth of reionisation  $\tau$  which is not unexpected when using CMB temperature data alone.  $\tau$  is also unconstrained when considering the model absent of a Bianchi component, thus for model comparison purposes an un-

constrained  $\tau$  does not pose any great concern. Indeed, for this simulation the model including a Bianchi component is favoured conclusively with a log-Bayes factor of  $\Delta \ln E \sim 50$ .

Partial-sky simulations are shown in Fig. 4. Since the covariance matrix  $\mathbf{X}(\Theta_C)$  is non-diagonal in this setting, the analysis is considerably more computationally demanding than the full-sky setting; hence, we set  $\ell_{\max} = 32$  in this simulation. The MAP estimated Bianchi VII<sub>h</sub> component is shown in Fig. 4(e) and clearly is an accurate estimate of the embedded component shown in Fig. 4(b) (note that the embedded Bianchi component was rotated such that the majority of its structure does not lie in the masked region). A noisy mask variance of  $\Sigma_m^2 = 100 (\text{mK})^2$  was adopted since numerical tests showed this effectively marginalised masked pixels in the data, while increasing  $\Sigma_m^2$  further had little impact. The marginalised posterior distributions recovered for each parameter

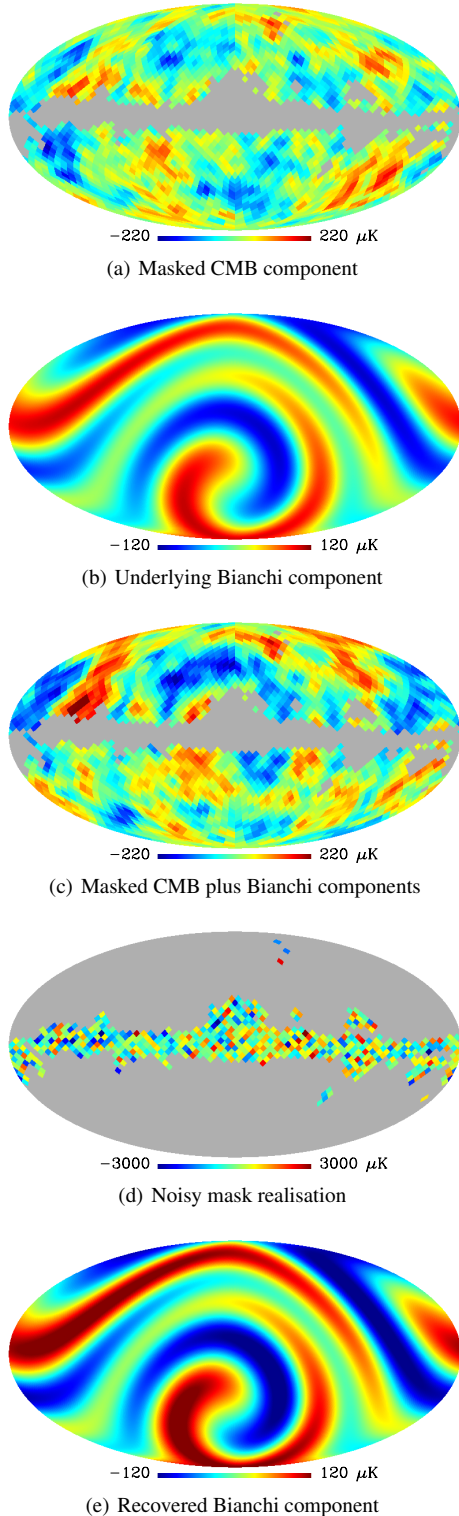


**Figure 4.** Partial-sky simulation at  $\ell_{\max} = 32$ . A Bianchi VII<sub>h</sub> component with a large amplitude is simulated (panel b) and embedded in a standard stochastic CMB map (panel a), yielding a resultant CMB plus Bianchi map (panel c) to which a mask, beam and noise are applied (the Bianchi component is rotated such that the majority of its structure does not lie in the masked region). A noisy mask (panel d) is added to the CMB plus Bianchi map and the partial-sky Bayesian analysis described in Sec. 3.3 is applied to recover a MAP estimated Bianchi component (panel e). The recovered Bianchi component (panel e) accurately estimates the embedded component (panel b).

are shown in Fig. 5. Both cosmological and Bianchi VII<sub>h</sub> parameters are estimated reasonably accurately, however since less data is now available due to the lower  $\ell_{\max}$  and masking, the marginalised posterior distributions are not as well constrained as the full-sky setting, as is to be expected.<sup>7</sup>

Reducing the maximum multipole considered has a large impact on the  $\Lambda$ CDM parameters determined by the acoustic peak positions and heights, but, thanks to the effective low- $\ell$  band-limit of the Bianchi VII<sub>h</sub> signal, affects the Bianchi VII<sub>h</sub> parameters much more mildly. This is clearly evident from the comparative behaviour of the posteriors for  $(\omega/H)_0$  and, e.g.,  $\Omega_c h^2$  or  $\Omega_b h^2$ . For model comparison purposes, this does not therefore pose any great concern. Indeed, for this simulation the model including a Bianchi component is also favoured conclusively with a log-Bayes factor of  $\Delta \ln E \sim 50$ . Nevertheless, by reducing  $\ell_{\max}$  we clearly discard a great deal of cosmologically interesting information. This can be recovered by calculating a high- $\ell$  likelihood assuming the Bianchi VII<sub>h</sub> contribution is zero for  $\ell > \ell_{\max}$ , using a conjugate-gradient-based implementation (Smith et al. 2007; Bennett et al. 2012) of the optimal, unbiased power-spectrum estimator (Tegmark 1997) in the presence of a mask. The two likelihoods can then be multiplied, assuming that the high- and low- $\ell$  data are independent. The implementation of such an algorithm for the simulations used here is unnecessary, as they are intended solely to validate the ANICOSMO code. When considering the WMAP data, we will use the purpose-built WMAP likelihood code<sup>8</sup> (Bennett et al. 2012), which implements the scheme described above, to calculate the high- $\ell$  likelihood and hence maximise the impact of the WMAP data.

The rationale for the simulations performed here is to validate the implementation of the ANICOSMO code, which has been demonstrated effectively in both the full- and partial-sky settings. Furthermore, although the details are not presented here, additional simulations were performed to validate the partial-sky setting. Two CMB maps were simulated with different cosmologies. A single hybrid map was then constructed with the Northern hemisphere given by the CMB simulated from the first cosmology and with the Southern hemisphere given by the CMB simulated from the second cosmology. ANICOSMO was applied to recover cosmological parameters from this hybrid map, once masking the Northern hemisphere and once masking the Southern hemisphere. In each of these tests the correct cosmology of the unmasked hemisphere was recovered, demonstrating that the partial-sky Bayesian analysis outlined in Sec. 3.3 effectively marginalises the masked pixels of the data. This test and the simulations described previously provide a strong validation of the ANICOSMO code in both the full- and partial-sky settings.

#### 4 ANALYSIS OF WMAP OBSERVATIONS

We analyse WMAP 9-year data for evidence of Bianchi VII<sub>h</sub> cosmologies, performing both the full- and partial-sky Bayesian analyses described in the preceding section. Firstly, we describe the

<sup>7</sup> Notice that the optical depth  $\tau$  appears to be better constrained in the partial-sky setting than in the full-sky setting. This is most likely a chance result for the particular simulations considered and is not expected to hold in general. Indeed, when considering the WMAP data (with the same  $\ell_{\max}$ ) the recovered posterior distributions for the optical depth are very similar (see Fig. 7 and Fig. 8).

<sup>8</sup> Available for download from [http://lambda.gsfc.nasa.gov/product/map/dr5/likelihood\\_get.cfm](http://lambda.gsfc.nasa.gov/product/map/dr5/likelihood_get.cfm).



specific full- and partial-sky WMAP data used and the cosmological models considered. We then present the results of our Bayesian analysis of Bianchi VII<sub>h</sub> models and place robust constraints on the vorticity of the Universe.

#### 4.1 Data

Previous searches for Bianchi VII<sub>h</sub> components embedded in WMAP data (e.g. Bridges et al. 2007) used full-sky data in the form of the ILC map to estimate the parameters of the Bianchi VII<sub>h</sub> model. While this greatly simplifies the form of the covariance matrix employed in the likelihood, the ILC map was not recommended for cosmological analysis (Eriksen et al. 2004) as it contains considerable foreground residuals, especially within the Galactic plane, and has a complex pixel noise structure. While these effects were ignored in previous studies (e.g. Bridges et al. 2007) since they are sub-dominant on the large scales of interest when studying Bianchi models, a better approach is to analyse partial-sky observations of individual WMAP frequency bands.

Our formalism, presented in Sec. 3.3, allows partial-sky data to be analysed for the first time in a statistically rigorous manner, minimising the residual contamination in the data and ensuring our conclusions are robust. We analyse the foreground-reduced WMAP 9-year W-band map (Bennett et al. 2012), masked with the conservative 9-year KQ75 sky cut (Bennett et al. 2012) to excise residual contamination. We select W-band data since this band, along with the V-band (which has lower resolution), suffers from the least foreground contamination (Bennett et al. 2012). The resulting data are shown in Fig. 6(a). In order to draw comparisons with previous studies we also analyse the full-sky WMAP 9-year ILC map (Bennett et al. 2012) shown in Fig. 6(b), under the proviso that any cosmological conclusions drawn from the ILC analysis must be treated with care.

Since Bianchi models have a low harmonic band-limit (see Fig. 1 of McEwen et al. 2006), we use only low- $\ell$  WMAP data in computing the Bianchi likelihood defined by Eqn. (4); specifically, we compute contributions to the likelihood of Eqn. (4) for  $\ell \leq \ell_{\max}^B = 32$ . For the partial-sky setting, where a non-diagonal covariance matrix must be inverted for each likelihood evaluation, a low band-limit  $\ell_{\max}^B$  is also convenient to reduce the computational cost of the analysis. The WMAP data so far described (the ILC map or the KQ75-masked W-band map in the full- and partial-sky settings respectively) are used for the Bianchi likelihood evaluation. As mentioned previously, we augment the low- $\ell$  Bianchi likelihood with the standard high- $\ell$  WMAP likelihood (Bennett et al. 2012) for  $\ell > \ell_{\max}^B = 32$ ; this likelihood function makes use of all WMAP temperature observations, as well as accurate beam models. The final log-likelihood is thus the sum of the low- $\ell$  Bianchi and high- $\ell$  9-year WMAP log-likelihood contributions (since the low- and high- $\ell$  data are essentially independent, the log-likelihood contributions can effectively be summed). As highlighted in Sec. 3.4, by including the high- $\ell$  WMAP likelihood we are able to constrain cosmological parameters to greater precision.

We incorporate approximate WMAP noise and beam effects in the low- $\ell$  Bianchi likelihood. Since the Bianchi likelihood is specified in harmonic space (due to the efficiency and accuracy for which Bianchi VII<sub>h</sub> models can be handled in harmonic space), we approximate the anisotropic WMAP noise by isotropic noise (which may be handled easily in harmonic space due to its diagonal covariance structure). We assume isotropic white noise specified by its power spectrum  $N_\ell = 0.015 (\mu\text{K})^2$  (computed by  $N_\ell = \Omega_{\text{pix}} \sigma_0^2 / \text{median}(N_{\text{obs}})$ , where  $N_{\text{obs}}$  is the W-band observation-

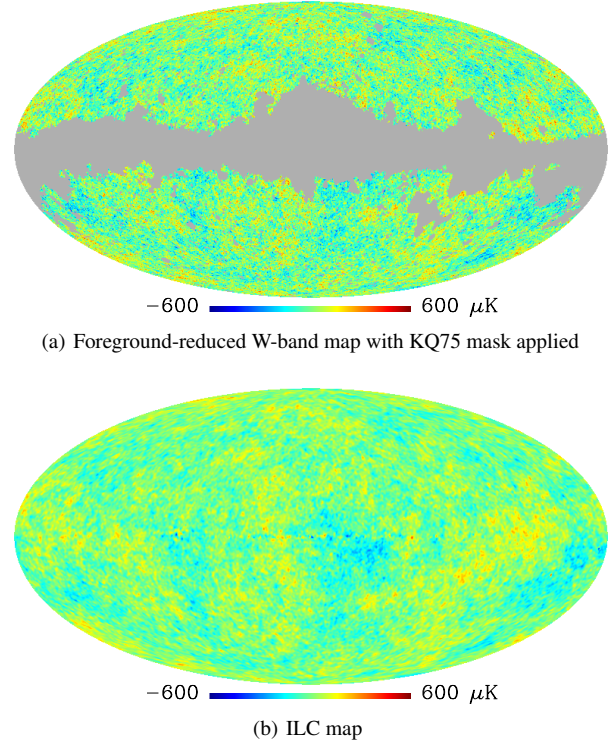


Figure 6. WMAP 9-year data analysed.

count map and  $\sigma_0 = 6544 \mu\text{K}$  is the W-band pixel noise level) and a Gaussian beam with FWHM of  $13.2'$  in order to approximate W-band observations accurately. As the individual WMAP bands are smoothed to a common resolution of  $1^\circ$  when creating the ILC (Bennett et al. 2012), we substitute a Gaussian beam of FWHM  $1^\circ$  when considering ILC data. Since we restrict to low- $\ell$  data for the Bianchi likelihood ( $\ell \leq \ell_{\max}^B = 32$ ), where WMAP noise and beam effects are sub-dominant, these approximations are accurate. For the high- $\ell$  contribution to the likelihood, the official WMAP 9-year likelihood is used, where noise and beams are modelled very accurately.

#### 4.2 Models

We consider three scenarios in this study: one physically motivated, and two phenomenological but motivated by previous analyses.

In the first (and only physically motivated) scenario, the Bianchi and cosmological parameters are coupled; i.e. the matter and dark-energy densities of the Bianchi and standard cosmological models are shared and thus identical. Since Bianchi VII<sub>h</sub> models are open (with flat models as the limiting case) we label this model the *open-coupled-Bianchi* model. When quoting final conclusions about Bianchi VII<sub>h</sub> cosmologies we will refer to this model since it is a physically well-motivated and consistent model.

It is also interesting to consider Bianchi CMB contributions arising from phenomenological models in which the Bianchi parameters are decoupled from the standard cosmological parameters; indeed, it is necessary to do so in order to compare to existing results, as this is the only approach employed in all previous analyses. In this non-physical scenario we consider a standard  $\Lambda\text{CDM}$  cosmology and a Bianchi VII<sub>h</sub> component with decoupled parameters (i.e. the total energy density of the standard cosmology and Bianchi cosmology may differ and are effectively separate param-

**Table 1.** The prior ranges used for the  $\Lambda$ CDM and Bianchi VII<sub>h</sub> parameters.

Parameter	Prior Range
$A_s$	$[1, 5] \times 10^{-9}$
$n_s$	[0.8, 1.1]
$\tau$	[0.082, 0.092]
$\Omega_b h^2$	[0.005, 0.05]
$\Omega_c h^2$	[0.05, 0.3]
$\Omega_\Lambda$	[0.5, 0.9]
$\Omega_k$	[0.001, 0.2]
$x$	[0.01, 1]
$(\omega/H)_0$	$[0, 1] \times 10^{-10}$
$\alpha$	[0, 360] <sup>o</sup>
$\beta$	[0, 180] <sup>o</sup>
$\gamma$	[0, 360] <sup>o</sup>
$\Omega_m^B$	[0, 0.99]
$\Omega_\Lambda^B$	[0, 0.99]

eters). As the  $\Lambda$ CDM cosmologies considered in previous analyses (e.g. Jaffe et al. 2005; Bridges et al. 2007) were flat, we similarly restrict our attention to flat  $\Lambda$ CDM components, and label this model the *flat-decoupled-Bianchi* model. Note that in this model we allow all  $\Lambda$ CDM parameters to vary.

Finally, we also consider the situation where the majority of the cosmological parameters are fixed and are not fitted simultaneously with the Bianchi VII<sub>h</sub> parameters. Following Bridges et al. (2007), we do allow the amplitude of the primordial power spectrum,  $A_s$ , to vary in this model, so that the amplitude of standard stochastic CMB temperature fluctuations is allowed to vary as we fit for an embedded Bianchi component. The remaining cosmological parameters are fixed at their values as constrained by WMAP 9-year observations, baryon acoustic oscillations and supernovae observations (Hinshaw et al. 2012). This is again a decoupled, non-physical scenario, and we label this model the *fixed-decoupled-Bianchi* model, where ‘fixed’ indicates that the standard cosmological parameters are essentially fixed.

For each of the three models discussed above, we consider models where a Bianchi VII<sub>h</sub> component is, and is not, included. Moreover, for the case where a Bianchi component is included, we consider both left-handed (LH) and right-handed (RH) Bianchi models, since the handedness of the coordinate system is also free in Bianchi VII<sub>h</sub> models. Consequently, we recover nine different models that we analyse (six models that include a Bianchi component and three that do not).

The prior ranges adopted on the  $\Lambda$ CDM and Bianchi parameters in this analysis are shown in Table 1, and are chosen conservatively to reflect our weak prior knowledge of the Bianchi models. The priors are uniform in all parameters of interest apart from the prior on the power spectrum amplitude,  $A_s$ , which is uniform in  $\log A_s$ , and the prior on the Euler angle  $\beta$ , which is uniform in  $\sin \beta$ . The priors on the Bianchi densities,  $\Omega_m^B$  and  $\Omega_\Lambda^B$ , are applied only in the decoupled models; in the coupled model these parameters are set by the sampled  $\Lambda$ CDM densities according to  $\Omega_m^B = \Omega_b + \Omega_c$  and  $\Omega_\Lambda^B = \Omega_\Lambda$ .

### 4.3 Results

We use WMAP 9-year data, as specified in Sec. 4.1, to study the Bianchi VII<sub>h</sub> models described in Sec. 4.2, using both the full- and partial-sky Bayesian analysis techniques presented in Sec. 3. We first consider the Bayes factors computed for different models, be-

**Table 2.** Log-Bayes factors computed for different models. The Bayes factor for each model is computed relative to the corresponding model that does not include a Bianchi component, where a positive Bayes factor favours the model that does include a Bianchi component.

Model	Full-sky ILC	Masked W-band
Open-coupled-Bianchi (LH)	$-0.3 \pm 0.2$	$0.0 \pm 0.2$
Open-coupled-Bianchi (RH)	$-0.3 \pm 0.2$	$0.1 \pm 0.2$
Flat-decoupled-Bianchi (LH)	$1.1 \pm 0.2$	$0.1 \pm 0.2$
Flat-decoupled-Bianchi (RH)	$0.1 \pm 0.2$	$0.1 \pm 0.2$
Fixed-decoupled-Bianchi (LH)	$1.7 \pm 0.1$	$0.6 \pm 0.1$
Fixed-decoupled-Bianchi (RH)	$0.6 \pm 0.1$	$0.3 \pm 0.1$

fore studying parameter estimates, best-fit maps, and finally vorticity bounds.

#### 4.3.1 Bayesian evidence

The log-Bayes factors computed for the different models considered are shown in Table 2. Neither left- nor right-handed open-coupled-Bianchi models are favoured by WMAP 9-year data, for either full-sky ILC data or partial-sky W-band data. Since this is the only physical model studied, we may already conclude that WMAP data do not favour a Bianchi VII<sub>h</sub> cosmology over the standard  $\Lambda$ CDM cosmology.

Nevertheless, we consider the other phenomenological models discussed in Sec. 4.2 where the Bianchi parameters are decoupled from the standard cosmological parameters, since these are the models that have been studied in previous analyses. For both the left-handed, flat-decoupled-Bianchi and fixed-decoupled-Bianchi models, we find evidence in favour of a Bianchi component (classified as significant on the Jeffreys scale), when analysing full-sky ILC data. However, when analysing masked W-band data we find no evidence for these models, suggesting that the evidence found in the full-sky setting is driven predominantly by ILC data near the Galactic plane. No evidence is found for the corresponding right-hand models.

#### 4.3.2 Parameter estimates

Although only left-handed, decoupled-Bianchi models show evidence for a Bianchi component when analysing full-sky ILC data, for completeness we show posterior distributions of the parameters of all left-handed models, using both full-sky ILC data and masked W-band data. We focus on left-handed models since neither dataset shows evidence for any right-handed models.

The posterior distributions of the parameters of the open-coupled-Bianchi model are shown in Fig. 7 for full- and partial-sky data. The standard cosmological parameters are relatively well constrained thanks to the high- $\ell$  WMAP likelihood (except for the optical depth to reionisation,  $\tau$ , as expected as only CMB temperature data are used). Since the constraints on the standard cosmological parameters are driven largely by the high- $\ell$  WMAP likelihood and are similar for all models, we do not comment on these further when discussing subsequent models. The Bianchi parameters, however, are typically poorly constrained for this model, especially for partial-sky W-band data. Furthermore, the Bianchi vorticity  $(\omega/H)_0$ , which traces the amplitude of the Bianchi-induced CMB temperature fluctuations, is peaked near zero. These posterior plots agree with the conclusion from the Bayesian evidence that WMAP 9-year data do not favour Bianchi VII<sub>h</sub> cosmologies.

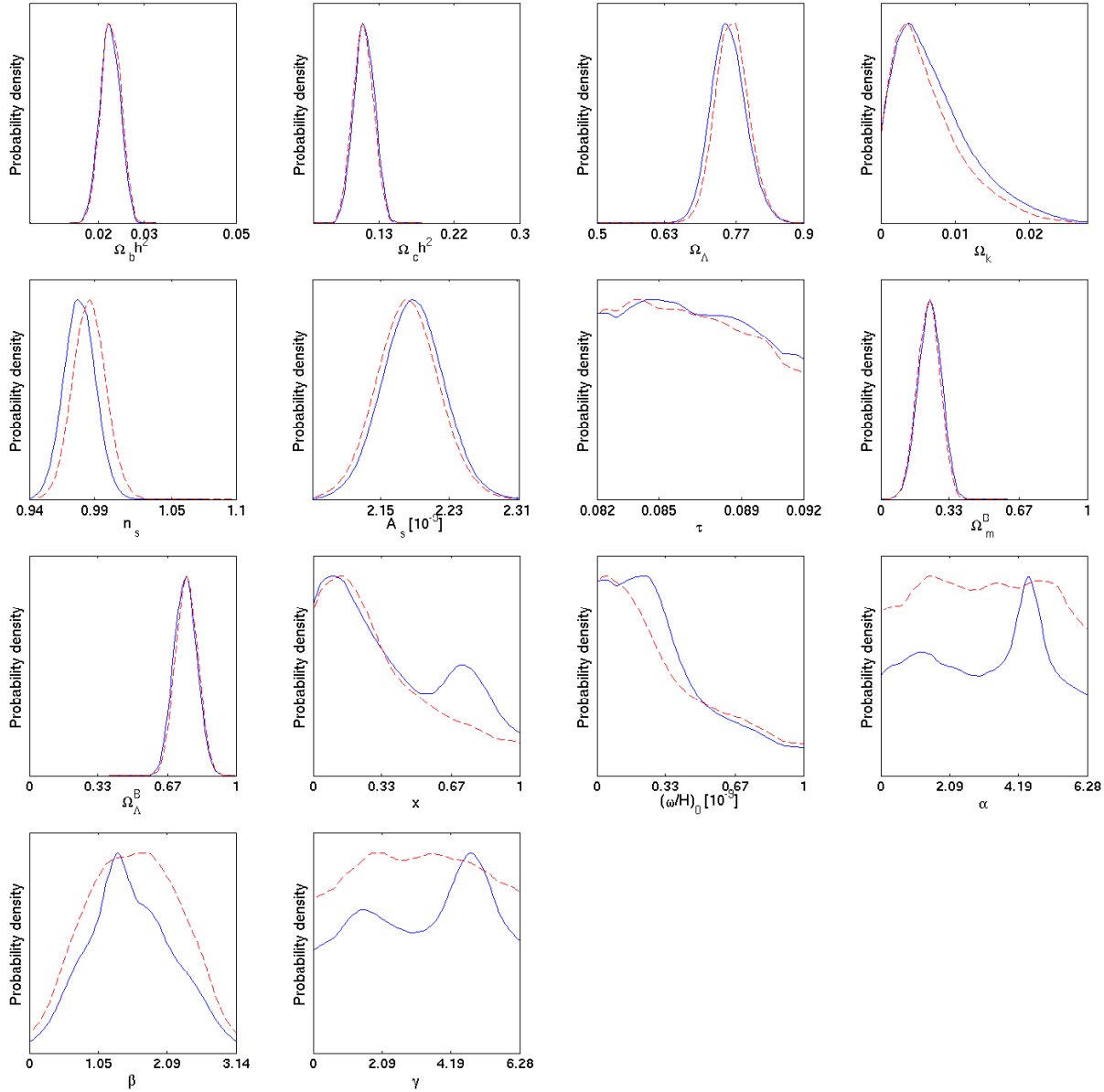


**Figure 7.** Posterior distributions for parameters of the left-handed open-coupled-Bianchi model computed from full-sky ILC data (solid blue curves) and Q75-masked W-band data (dashed red curves).

The posterior distributions of the parameters of the flat-decoupled-Bianchi model are shown in Fig. 8 for full- and partial-sky data. For the full-sky analysis, the Bianchi parameters are relatively well-constrained (except for  $\Omega_\Lambda^B$  due to the  $\Omega_m^B - \Omega_\Lambda^B$  degeneracy of Bianchi VII<sub>h</sub> models), agreeing with the previous inference from the Bayesian evidence that a Bianchi component is favoured in this setting. Bianchi parameters are not well constrained for partial-sky data and, moreover, the Bianchi vorticity  $(\omega/H)_0$  is peaked near zero, agreeing with the conclusion that partial-sky data do not favour a Bianchi component.

The posterior distributions of the parameters of the fixed-decoupled-Bianchi model are shown in Fig. 9 for full- and partial-sky data. The conclusions drawn from the posterior distributions of the parameters of this model are identical to the flat-decoupled-Bianchi model: essentially, the Bianchi parameters are well constrained when full-sky ILC data are used, but not when partial-sky

data are used. Again, these findings agree with conclusions drawn previously using the Bayesian evidence.

Finally, we summarise the parameter estimates made from the joint posterior distribution  $P(\Theta | \mathbf{d}, M)$  for each model in Table 3 and Table 4, for partial- and full-sky data respectively. We compute both maximum *a-posteriori* (MAP) parameter estimates from the peak of the joint posterior distribution and estimates from the mean of the marginalised posterior distribution for each parameter. One-standard-deviation errors are also quoted for the mean-posterior parameter estimates.

#### 4.3.3 Best-fit maps

For the two models where the Bayes factor provides significant evidence in support of a Bianchi component (see Table 2), namely the non-physical flat-decoupled-Bianchi and fixed-decoupled-Bianchi

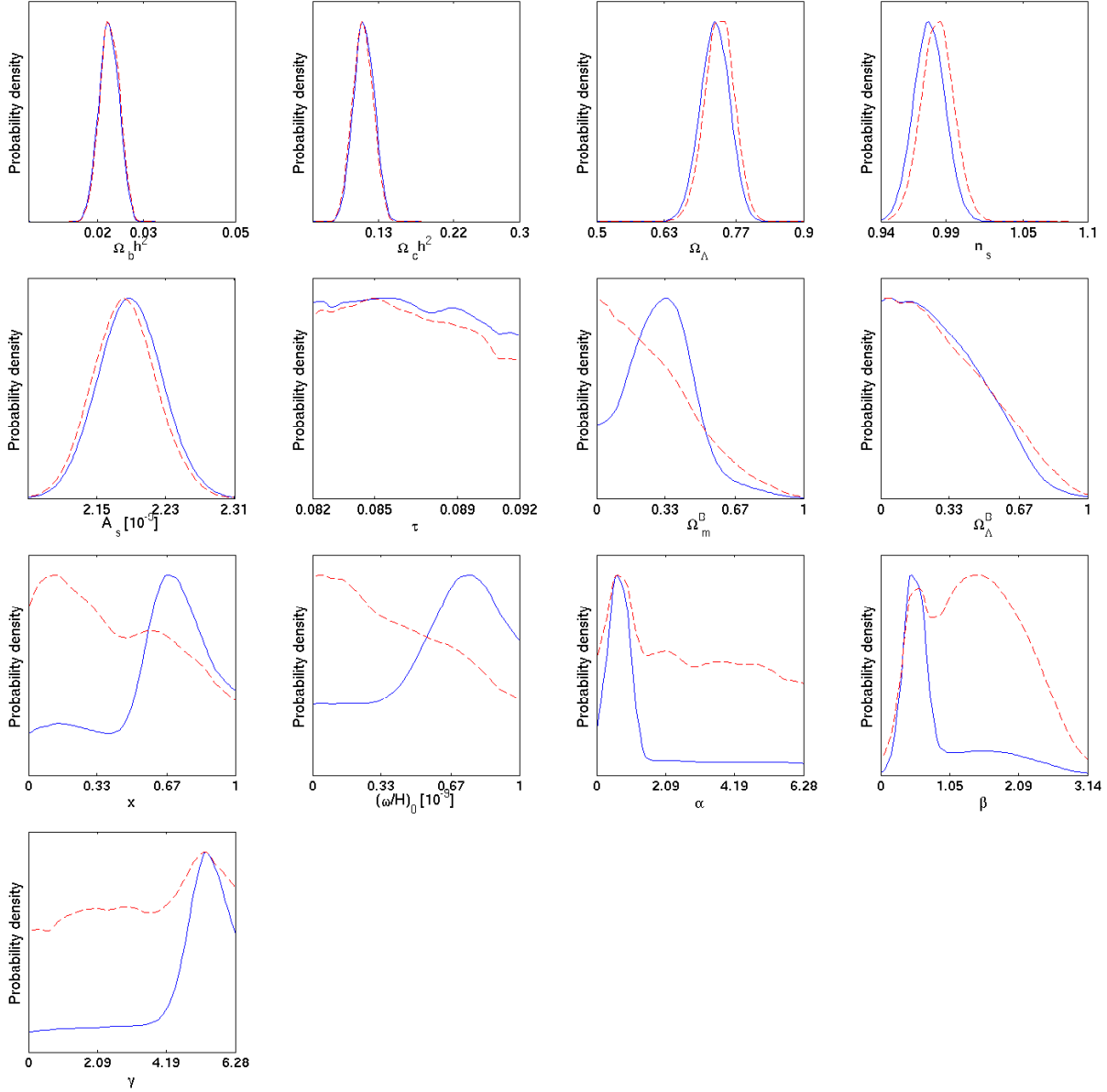


**Figure 8.** Posterior distributions for parameters of the left-handed flat-decoupled-Bianchi model computed from full-sky ILC data (solid blue curves) and Q75-masked W-band data (dashed red curves).

models, we plot the best-fit embedded Bianchi maps in Fig. 10(a) and Fig. 10(b), respectively. Best-fit maps are computed from the MAP parameter estimates contained in Table 3. These best-fit maps are very similar to those found in previous releases of WMAP data (Jaffe et al. 2005; Bridges et al. 2007).

#### 4.3.4 Vorticity bounds

We conclude our analysis of WMAP 9-year data by reiterating that only the open-coupled-Bianchi model is physical. The other models considered are non-physical since the Bianchi parameters are decoupled from the standard cosmological parameters: the Bianchi component can therefore require parameters, for example, a total energy density, that are incompatible with the stochastic CMB component. For the physical open-coupled-Bianchi model no evidence for a Bianchi component is found in either full-sky ILC or partial-

sky W-band data. In this physical model we can therefore place constraints on the vorticity of Bianchi VII<sub>h</sub> cosmologies. For full-sky ILC data we recover the constraint  $(\omega/H)_0 < 8.1 \times 10^{-10}$  at 95% confidence, for both left- and right-handed models. For partial-sky W-band data we recover the constraint  $(\omega/H)_0 < 8.1 \times 10^{-10}$  for the left-handed model and the constraint  $(\omega/H)_0 < 8.6 \times 10^{-10}$  for the right-handed model, both at 95% confidence. These constraints on the global anisotropy of our Universe are placed in the context of a well-motivated, physical model, namely Bianchi VII<sub>h</sub> cosmologies, using robust Bayesian statistical methods.

## 5 CONCLUSIONS

We have performed a definitive analysis of Bianchi VII<sub>h</sub> cosmologies with WMAP 9-year temperature data. We have studied full-sky ILC data and masked W-band data, using Bayesian analysis tech-

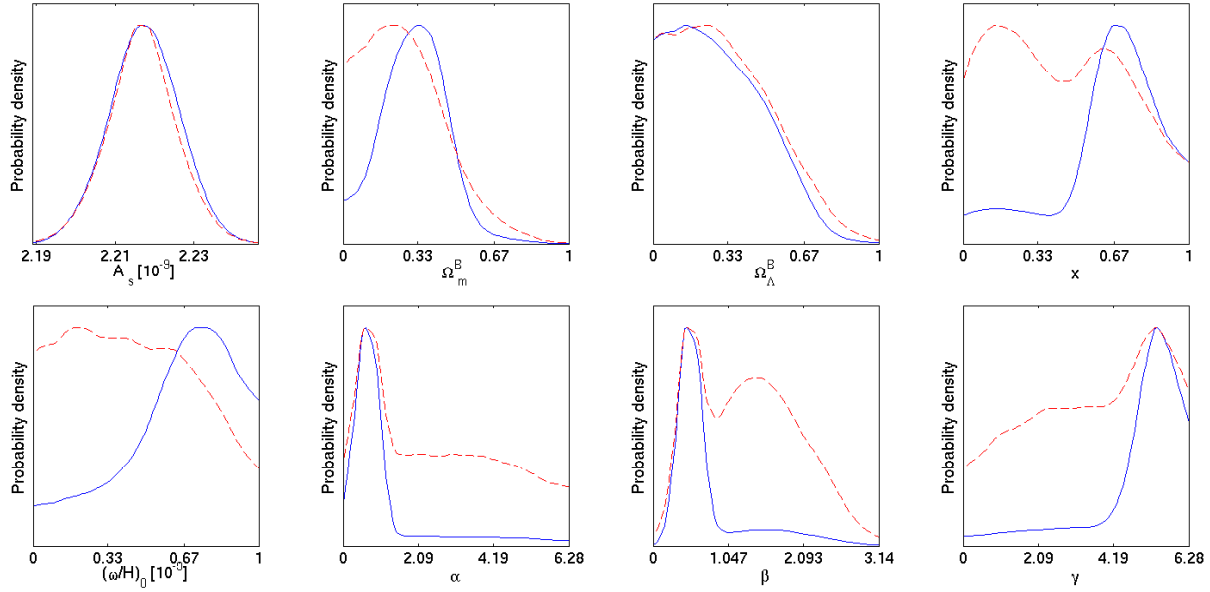


**Figure 9.** Posterior distributions for parameters of the left-handed fixed-decoupled-Bianchi model computed from full-sky ILC data (solid blue curves) and KQ75-masked W-band data (dashed red curves).

**Table 3.** Parameter estimates recovered for various left-handed models from full-sky ILC data. Note that some of these models are not favoured by the Bayesian evidence and some parameters are not well constrained. We nevertheless show all parameter estimates for completeness.

Parameter	Open-coupled-Bianchi		Flat-decoupled-Bianchi		Fixed-decoupled-Bianchi	
	MAP	Mean	MAP	Mean	MAP	Mean
$A_s$	$2.21 \times 10^{-9}$	$(2.19 \pm 0.03) \times 10^{-9}$	$2.17 \times 10^{-9}$	$(2.19 \pm 0.04) \times 10^{-9}$	$2.219 \times 10^{-9}$	$(2.217 \pm 0.009) \times 10^{-9}$
$n_s$	0.98	$0.98 \pm 0.01$	0.98	$0.98 \pm 0.01$	—	—
$\tau$	0.084	$0.087 \pm 0.003$	0.084	$0.087 \pm 0.003$	—	—
$\Omega_b h^2$	0.023	$0.0226 \pm 0.0004$	0.023	$0.0225 \pm 0.0004$	—	—
$\Omega_c h^2$	0.12	$0.112 \pm 0.004$	0.11	$0.112 \pm 0.004$	—	—
$\Omega_\Lambda$	0.72	$0.75 \pm 0.03$	0.74	$0.73 \pm 0.02$	—	—
$\Omega_k$	0.002	$0.007 \pm 0.005$	—	—	—	—
$\Omega_m^B$	0.27	$0.24 \pm 0.03$	0.3	$0.3 \pm 0.2$	0.4	$0.3 \pm 0.1$
$\Omega_\Lambda^B$	0.72	$0.75 \pm 0.03$	0.3	$0.3 \pm 0.2$	0.2	$0.3 \pm 0.2$
$x$	0.3	$0.4 \pm 0.3$	0.7	$0.6 \pm 0.2$	0.6	$0.6 \pm 0.2$
$(\omega/H)_0$	$8 \times 10^{-10}$	$(3 \pm 2) \times 10^{-10}$	$10 \times 10^{-10}$	$(6 \pm 3) \times 10^{-10}$	$9 \times 10^{-10}$	$(6 \pm 2) \times 10^{-10}$
$\alpha$	$2.5^\circ$	$181.8^\circ \pm 100.1^\circ$	$41.3^\circ$	$88.8^\circ \pm 90.0^\circ$	$41.0^\circ$	$71.2^\circ \pm 73.7^\circ$
$\beta$	$122.5^\circ$	$87.9^\circ \pm 35.7^\circ$	$27.2^\circ$	$50.8^\circ \pm 36.4^\circ$	$27.6^\circ$	$43.6^\circ \pm 30.9^\circ$
$\gamma$	$242.5^\circ$	$189.7^\circ \pm 100.9^\circ$	$319.8^\circ$	$259.9^\circ \pm 90.1^\circ$	$314.1^\circ$	$277.7^\circ \pm 75.6^\circ$

**Table 4.** Parameter estimates recovered for various left-handed models from KQ75-masked W-band data. Note that these models are not favoured by the Bayesian evidence and some parameters are not well constrained. We nevertheless show all parameter estimates for completeness.

Parameter	Open-coupled-Bianchi		Flat-decoupled-Bianchi		Fixed-decoupled-Bianchi	
	MAP	Mean	MAP	Mean	MAP	Mean
$A_s$	$2.17 \times 10^{-9}$	$(2.18 \pm 0.04) \times 10^{-9}$	$2.19 \times 10^{-9}$	$(2.18 \pm 0.04) \times 10^{-9}$	$2.226 \times 10^{-9}$	$(2.217 \pm 0.008) \times 10^{-9}$
$n_s$	0.98	$0.99 \pm 0.01$	0.98	$0.98 \pm 0.01$	—	—
$\tau$	0.084	$0.087 \pm 0.003$	0.084	$0.087 \pm 0.003$	—	—
$\Omega_b h^2$	0.023	$0.0228 \pm 0.0005$	0.023	$0.0227 \pm 0.0004$	—	—
$\Omega_c h^2$	0.11	$0.110 \pm 0.004$	0.11	$0.111 \pm 0.004$	—	—
$\Omega_\Lambda$	0.75	$0.76 \pm 0.03$	0.73	$0.74 \pm 0.02$	—	—
$\Omega_k$	0.003	$0.007 \pm 0.005$	—	—	—	—
$\Omega_m^B$	0.25	$0.23 \pm 0.03$	0.3	$0.3 \pm 0.2$	0.1	$0.3 \pm 0.2$
$\Omega_\Lambda^B$	0.75	$0.76 \pm 0.03$	0.4	$0.3 \pm 0.2$	0.4	$0.3 \pm 0.2$
$x$	0.5	$0.3 \pm 0.3$	0.7	$0.4 \pm 0.3$	0.2	$0.5 \pm 0.3$
$(\omega/H)_0$	$6 \times 10^{-10}$	$(3 \pm 3) \times 10^{-10}$	$8 \times 10^{-10}$	$(4 \pm 3) \times 10^{-10}$	$4 \times 10^{-10}$	$(4 \pm 3) \times 10^{-10}$
$\alpha$	$55.6^\circ$	$179.0^\circ \pm 101.0^\circ$	$37.0^\circ$	$162.8^\circ \pm 104.3^\circ$	$244.0^\circ$	$150.2^\circ \pm 102.5^\circ$
$\beta$	$59.3^\circ$	$90.6^\circ \pm 38.3^\circ$	$26.4^\circ$	$82.1^\circ \pm 39.6^\circ$	$106.9^\circ$	$75.3^\circ \pm 39.0^\circ$
$\gamma$	$102.6^\circ$	$180.5^\circ \pm 100.3^\circ$	$321.0^\circ$	$193.2^\circ \pm 103.8^\circ$	$170.3^\circ$	$203.8^\circ \pm 100.3^\circ$

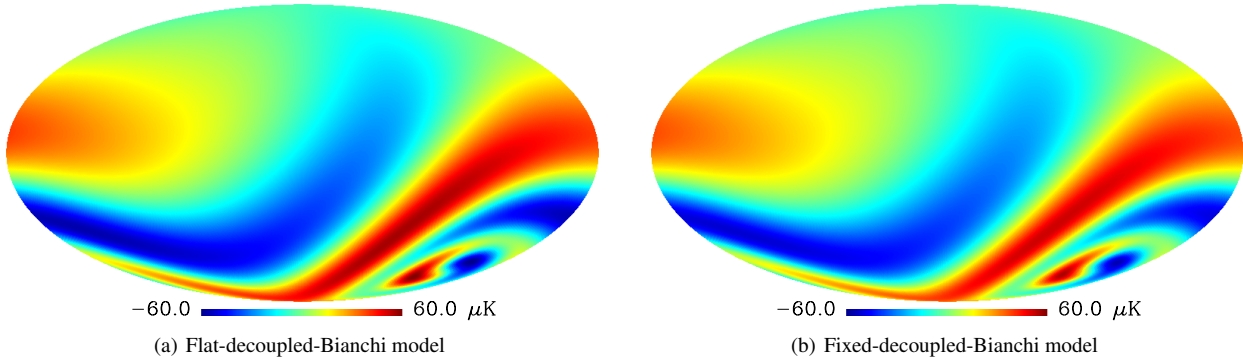


**Figure 10.** Best-fit non-physical Bianchi  $\text{VII}_h$  templates found in full-sky ILC data.

niques developed for the full- and partial-sky settings. Three different models were studied, namely the physically motivated open-coupled-Bianchi model, where the Bianchi and standard cosmological parameters are coupled, and the flat-decoupled-Bianchi and fixed-decoupled-Bianchi models, which are non-physical since the Bianchi and standard cosmological parameters are decoupled. Although we have focused here on Bianchi models, our analysis techniques may be easily extended to study other anisotropic cosmologies such as non-trivial topologies; such models will be the focus of future research.

For the non-physical decoupled models, we find Bayesian evidence favouring the inclusion of a left-handed Bianchi component when analysing full-sky ILC data. The resulting best-fit Bianchi maps found in WMAP 9-year data are similar to those found in previous releases of WMAP data (Jaffe et al. 2005; Bridges et al. 2007). However, when studying these models with masked W-band data we find no evidence for a Bianchi component, suggesting that data near the Galactic plane provide a large contribution to the evidence found in the full-sky setting.

For the physical Bianchi  $\text{VII}_h$  model, we find no evidence for the inclusion of a Bianchi component in either full- or partial-sky WMAP data. Since this is a well-motivated, physical model we can state definitively that WMAP data do not favour Bianchi  $\text{VII}_h$  cosmologies over  $\Lambda\text{CDM}$ . However, neither is it possible to conclusively discount Bianchi  $\text{VII}_h$  cosmologies in favour of  $\Lambda\text{CDM}$  cosmologies. We constrain the vorticity of Bianchi  $\text{VII}_h$  cosmologies, and hence the large-scale anisotropy of the universe, at  $(\omega/H)_0 < 8.6 \times 10^{-10}$  with 95% confidence.

Bianchi  $\text{VII}_h$  cosmologies induce a global anisotropic CMB temperature contribution that is inherently low-resolution, so the higher resolution of forthcoming *Planck* (Planck collaboration 2005) data as compared to WMAP is not in itself relevant to enhanced constraints on these models. However, *Planck*'s ability to remove large-scale astrophysical foregrounds will result in CMB observations of unprecedented precision over almost the entire sky. An analysis of Bianchi  $\text{VII}_h$  cosmologies using *Planck* temperature data will thus be very informative. Moreover, polarised *Planck* observations will also have the potential to further constrain Bianchi  $\text{VII}_h$  cosmologies.

#### ACKNOWLEDGEMENTS

We thank Anthony Challinor for useful discussions about masking in harmonic space. JDM is supported in part by a Newton International Fellowship from the Royal Society and the British

Academy. TJ was supported by STFC during the course of this work. SMF is supported by STFC and a grant from the Foundational Questions Institute (FQXi) Fund, a donor-advised fund of the Silicon Valley Community Foundation on the basis of proposal FQXi-RFP3-1015 to the Foundational Questions Institute. HVP is supported by STFC, the Leverhulme Trust, and the European Research Council under the European Community's Seventh Framework Programme (FP7/2007- 2013) / ERC grant agreement no 306478-CosmicDawn. We acknowledge use of the following public software packages: HEALPix (Górski et al. 2005); CAMB (Lewis et al. 2000); MultiNest (Feroz & Hobson 2008; Feroz et al. 2009); BIANCHI2 (McEwen et al. 2006); S2 (McEwen et al. 2007). We acknowledge use of the Legacy Archive for Microwave Background Data Analysis (LAMBDA). Support for LAMBDA is provided by the NASA Office of Space Science. The authors acknowledge the use of the UCL Legion High Performance Computing Facility (Legion@UCL), and associated support services, in the completion of this work.

#### REFERENCES

- Barrow J.D., 1986, *Canadian Journal of Physics*, 64, 152  
 Barrow J.D., Juszkiewicz R., Sonoda D.H., 1985, *Mon. Not. Roy. Astron. Soc.*, 213, 917  
 Bennett C.L., et al., 2003, *Astrophys. J. Supp.*, 148, 1, [astro-ph/0302207](#)  
 Bennett C.L., et al., 2012, ArXiv e-prints, [1212.5225](#)  
 Bielewicz P., Riazuelo A., 2009, *Mon. Not. Roy. Astron. Soc.*, 396, 609, [0804.2437](#)  
 Bridges M., McEwen J.D., Cruz M., Hobson M.P., Lasenby A.N., Vielva P., Martínez-González E., 2008, *Mon. Not. Roy. Astron. Soc.*, 390, 4, 1372, [arXiv:0712.1789](#)  
 Bridges M., McEwen J.D., Lasenby A.N., Hobson M.P., 2007, *Mon. Not. Roy. Astron. Soc.*, 377, 1473, [astro-ph/0605325](#)  
 Bunn E.F., Ferreira P.G., Silk J., 1996, *Phys. Rev. Lett.*, 77, 2883, [astro-ph/9605123](#)  
 Cayon L., Banday A.J., Jaffe T., Eriksen H.K., Hansen F.K., Górski K.M., Jin J., 2006, ArXiv, [astro-ph/0602023](#)  
 Collins C.B., Hawking S.W., 1973, *Mon. Not. Roy. Astron. Soc.*, 162, 307  
 Cornish N.J., Spergel D.N., Starkman G.D., Komatsu E., 2004, *Phys. Rev. Lett.*, 92, 20, 201302, [arXiv:astro-ph/0310233](#)  
 Cruz M., Tucci M., Martínez-González E., Vielva P., 2006, *Mon. Not. Roy. Astron. Soc.*, 369, 57, [astro-ph/0601427](#)

- Dineen P., Rocha G., Coles P., 2005, *Mon. Not. Roy. Astron. Soc.*, 358, 1285, [astro-ph/0404356](#)
- Eriksen H.K., Banday A.J., Górski K.M., Lilje P.B., 2004, *Astrophys. J.*, 612, 633, [astro-ph/0403098](#)
- Feroz F., Hobson M.P., 2008, *Mon. Not. Roy. Astron. Soc.*, 384, 449, [0704.3704](#)
- Feroz F., Hobson M.P., Bridges M., 2009, *Mon. Not. Roy. Astron. Soc.*, 398, 1601, [0809.3437](#)
- Ghosh T., Hajian A., Souradeep T., 2007, *Phys. Rev. D.*, 75, 8, 083007, [arXiv:astro-ph/0604279](#)
- Górski K.M., Hivon E., Banday A.J., Wandelt B.D., Hansen F.K., Reinecke M., Bartelmann M., 2005, *Astrophys. J.*, 622, 759, [astro-ph/0409513](#)
- Hinshaw G., et al., 2003, *Astrophys. J. Supp.*, 148, 135, [arXiv:astro-ph/0302217](#)
- Hinshaw G., et al., 2012, *ArXiv e-prints*, [1212.5226](#)
- Hivon E., Górski K.M., Netterfield C.B., Crill B.P., Prunet S., Hansen F., 2002, *Astrophys. J.*, 567, 2, [arXiv:astro-ph/0105302](#)
- Jaffe T.R., Banday A.J., Eriksen H.K., Górski K.M., Hansen F.K., 2005, *Astrophys. J. Lett.*, 629, L1, [astro-ph/0503213](#)
- Jaffe T.R., Banday A.J., Eriksen H.K., Gorski K.M., Hansen F.K., 2006a, *ArXiv*, [astro-ph/0606046](#)
- Jaffe T.R., Banday A.J., Eriksen H.K., Górski K.M., Hansen F.K., 2006b, *Astrophys. J.*, 643, 616, [astro-ph/0603844](#)
- Jaffe T.R., Hervik S., Banday A.J., Górski K.M., 2006c, *Astrophys. J.*, 644, 701, [astro-ph/0512433](#)
- Jeffreys H., 1961, *Theory of probability*, Oxford University Press, Oxford, 3rd edition
- Kogut A., Hinshaw G., Banday A.J., 1997, *Phys. Rev. D.*, 55, 1901, [astro-ph/9701090](#)
- Komatsu E., et al., 2011, *Astrophys.J.Supp.*, 192, 18, [arXiv:1001.4538](#)
- Kunz M., Aghanim N., Cayon L., Forni O., Riazuelo A., et al., 2006, *Phys. Rev. D.*, D73, 023511, [astro-ph/0510164](#)
- Land K., Magueijo J., 2006, *Mon. Not. Roy. Astron. Soc.*, 367, 1714, [astro-ph/0509752](#)
- Larson D., et al., 2011, *Astrophys. J. Supp.*, 192, 16, [1001.4635](#)
- Lewis A., Challinor A., Lasenby A., 2000, *Astrophys. J.*, 538, 473, [astro-ph/9911177](#)
- McEwen J.D., Hobson M.P., Lasenby A.N., Mortlock D.J., 2006, *Mon. Not. Roy. Astron. Soc.*, 369, 1858, [astro-ph/0510349](#)
- McEwen J.D., Hobson M.P., Mortlock D.J., Lasenby A.N., 2007, *IEEE Trans. Sig. Proc.*, 55, 2, 520, [astro-ph/0506308](#)
- Niarchou A., Jaffe A.H., Pogossian L., 2003, *Phys. Rev. D.*, 69, 063515
- Page L., et al., 2007, *Astrophys. J. Supp.*, 170, 335, [arXiv:astro-ph/0603450](#)
- Planck collaboration, 2005, *ESA Planck blue book*, Technical Report ESA-SCI(2005)1, ESA, [astro-ph/0604069](#)
- Pontzen A., 2009, *prd*, 79, 10, 103518, [0901.2122](#)
- Pontzen A., Challinor A., 2007, *Mon. Not. Roy. Astron. Soc.*, 380, 1387, [0706.2075](#)
- Pontzen A., Challinor A., 2011, *Classical and Quantum Gravity*, 28, 18, 185007, [1009.3935](#)
- Skilling J., 2004, in R. Fischer, R. Preuss, U.V. Toussaint, editors, *American Institute of Physics Conference Series*, volume 735 of *American Institute of Physics Conference Series*, 395–405
- Smith K.M., Zahn O., Doré O., 2007, *Phys. Rev. D.*, 76, 4, 043510, [0705.3980](#)
- Tegmark M., 1997, *Phys. Rev. D.*, 55, 5895, [arXiv:astro-ph/9611174](#)
- Verde L., et al., 2003, *Astrophys. J. Supp.*, 148, 195, [astro-ph/0302218](#)
- Vielva P., 2010, *Advances in Astronomy*, 2010, 592094, [1008.3051](#)
- Vielva P., Martínez-González E., Barreiro R.B., Sanz J.L., Cayón L., 2004, *Astrophys. J.*, 609, 22, [astro-ph/0310273](#)